# Reassessment of Focal Depths of Shallow Moderate-Sized Earthquakes in Mariana Subduction Zone with Short-Period Rayleigh-Wave Amplitude Spectra

Gaohua Zhu[*1,2], Hongzhao Xi[1,2,3], Zhenteng Wang[1,2,3], Yi Wang[4], Xiaohui He[5], and Hongfeng Yang[6]

## Abstract

**Focal depths provide vital information for seismogenic mechanisms and tectonic structures. Because of sparse seismic stations in the Mariana subduction zone, accurately determining the focal depth of shallow earthquakes is challenging. The amplitude spectra of short-period Rayleigh waves are highly depth sensitive and are applicable at local and regional distances with sparse seismic station coverage. In this study, we collect seismic data at local and regional distances in the Mariana region, and then use the optimal period of short-period Rayleigh-wave amplitude spectra to determine the depths of shallow moderate-sized earthquakes. The difference between our resolved depths and the Incorporated Research Institutions for Seismology (IRIS) results ranges from −12.5 to 17.5 km, whereas the difference between our resolved depths and the Global Centroid Moment Tensor (Global CMT) depths has a range of −7.5 to 12.5 km. To further verify the estimated source depth, we used depth phase modeling to constrain the source depth of the largest $M_w$ 5.9 earthquake. The result of depth phase modeling (27.9 ± 0.3 km) is slightly larger than the depth of 24.4 ± 1.4 km using the optimal period method. In comparison, the estimated depth is quite different from the fixed values of 10 and 12 km in the IRIS and Global CMT catalogs, respectively. The study demonstrates the efficacy of this approach on shallow offshore earthquakes and the need to reassess the depth of earthquakes in the Mariana subduction zone.**

**Cite this article as** Zhu, G., H. Xi, Z. Wang, Y. Wang, X. He, and H. Yang (2026). Reassessment of Focal Depths of Shallow Moderate-Sized Earthquakes in Mariana Subduction Zone with Short-Period Rayleigh-Wave Amplitude Spectra, *Seismol. Res. Lett.* **XX**, 1–11, doi: 10.1785/0220260037.

**Supplemental Material**

## Introduction

Focal depth is crucial for understanding the seismogenic mechanisms, investigating the kinematics and dynamics of faults and the Earth's interior structure. In subduction zones, the precise locations of earthquakes provide implications for the plate interface (Emry *et al.*, 2011; Wang *et al.*, 2024), slab morphology (Hayes *et al.*, 2018), and fluid activities (Peng *et al.*, 2024; Suzuki *et al.*, 2025), which likely control frictional properties and rupture behavior along a plate interface (Wang and He, 2008). In outer-rise regions of the incoming plate, earthquake focal depth can be an indicator of the depth of extensional faulting and the neutral plane of the subducting plate (Craig *et al.*, 2014; Chen *et al.*, 2022; Qian *et al.*, 2024). The Mariana subduction zone is located in the western Pacific, adjacent to the Eurasian continent (Fig. 1). It is an unusual subduction zone with an old, steep subducting Pacific plate and the deepest trench on Earth, creating a unique geological environment (Stern *et al.*, 2003). Because of the paucity of local seismic stations in the Mariana subduction zone, accurately determining the location of earthquakes is challenging, especially the focal depth of shallow earthquakes. It is considered that far distance stations (distance > 1.4 times the focal depth) have limited constraints on focal depth (Gomberg *et al.*, 1990). This leads to large location uncertainties (up to tens of kilometers) for historical earthquakes along the Mariana subduction zone (Emry *et al.*, 2011). In global catalogs, a significant

1. Key Laboratory of Ocean Observation and Forecasting, Institute of Oceanology, Chinese Academy of Sciences, Qingdao, China, https://orcid.org/0000-0003-4186-7375 (GZ); https://orcid.org/0009-0003-2972-4141 (HX); 2. Laboratory of Marine Geology and Environment, Institute of Oceanology, Chinese Academy of Sciences, Qingdao, China; 3. University of Chinese Academy of Sciences, Beijing, China; 4. Innovation Academy for Precision Measurement Science and Technology, China Academy of Sciences, Wuhan, China, https://orcid.org/0000-0002-2037-1381 (YW); 5. Guangdong Provincial Key Laboratory of Geodynamics and Geohazards, School of Earth Sciences and Engineering, Sun Yat-sen University, Zhuhai, China, https://orcid.org/0000-0001-8609-4105 (XH); 6. Department of Earth and Environmental Sciences, The Chinese University of Hong Kong, Hong Kong, China, https://orcid.org/0000-0002-5925-6487 (HY)

*Corresponding author: zhugaohua@qdio.ac.cn

© Seismological Society of America



Downloaded from pubs.geoscienceworld.org/ssa/srl/article-pdf/doi/10.1785/0220260037/8402433/srl-2026037.1.pdf by Chinese University Hong Kong user on 17 October 2026

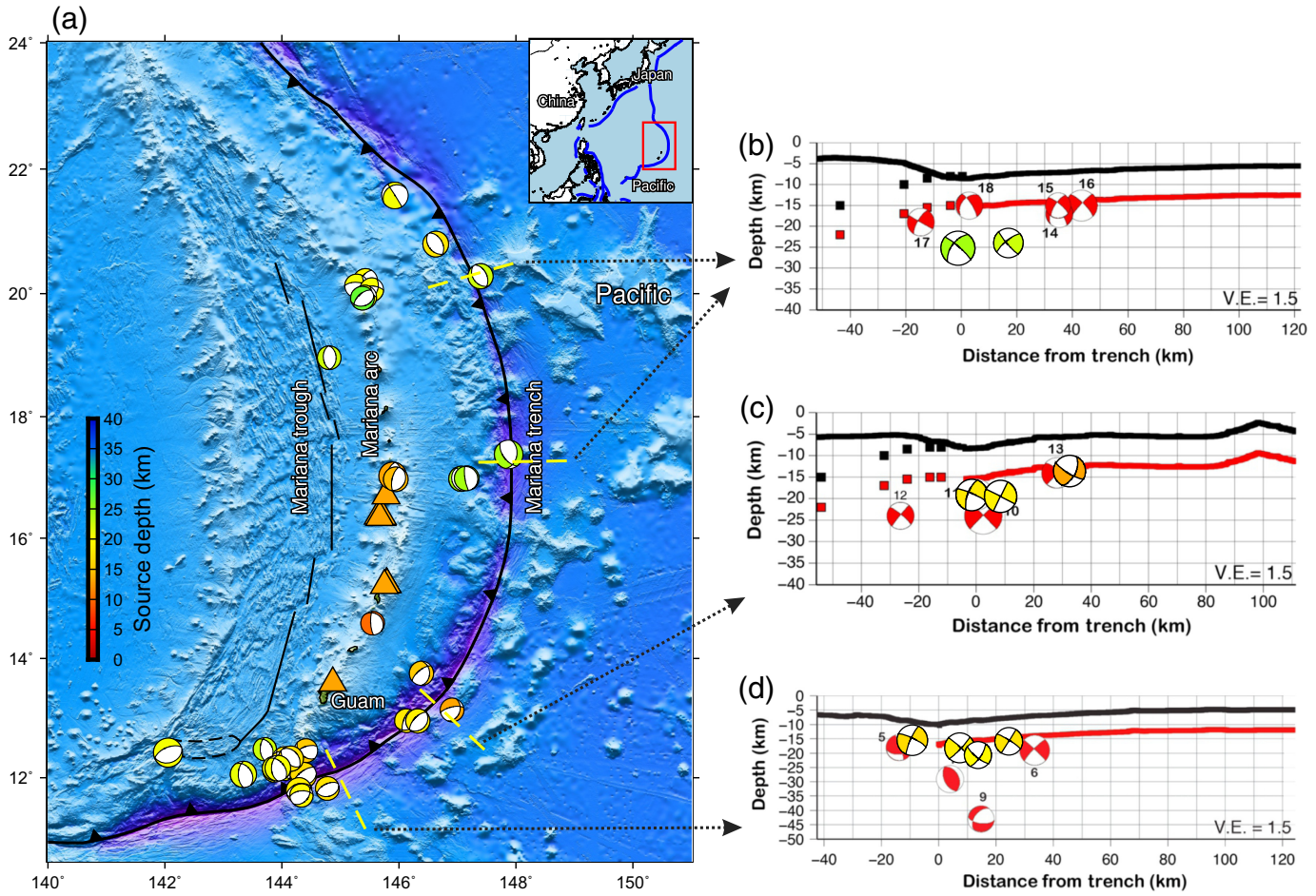



**Figure 1.** Location of the analyzed earthquakes (shown as focal mechanism plots) in this study. (a) Map view of earthquakes colored by estimated source depth using optimal period of Rayleigh-wave amplitude spectra. The orange triangles represent the available seismic stations. The yellow-dashed lines show the locations of profiles. Inset shows the location of the study area (red frame). (b–d) Projections of near-trench earthquakes on the adjacent trench perpendicular profiles. The base map and the red–white focal mechanisms with numbers on top are adopted from Emry *et al.* (2014). The thick black and red lines show the bathymetry and Moho, respectively. Black and red squares indicate the plate interface and continuous Moho, respectively. The color version of this figure is available only in the electronic edition.

portion of shallow seismic events is typically assigned a fixed depth of 10 km in the region (Table S1, available in the supplemental material to this article).

Significant efforts have been made to improve the precision of earthquake locations through the deployment of local ocean-bottom seismograph (OBS) observations in the Mariana region. The local OBS recordings provide opportunities for investigating many smaller earthquakes with higher location precision, which shed light on the characteristics of the Mariana subduction zone. For example, extensional earthquakes with depths of 30–35 km below the seafloor are recorded by OBS in central (Eimer *et al.*, 2020) and southern Mariana (Chen *et al.*, 2022), indicating that the incoming plate mantle may experience significant hydration to depths of 30–40 km below the seafloor near the trench axis at the central (Cai *et al.*, 2018; Eimer *et al.*, 2020; Mark *et al.*, 2023) and southern Mariana trench (Zhu *et al.*, 2021; He *et al.*, 2025; Zhang *et al.*, 2024, 2025). Unfortunately, OBS experiments are only carried out in certain periods (from months to a year) in the central (Shiobara *et al.*, 2010; Emry *et al.*, 2011; Barklage *et al.*, 2015; Eimer *et al.*, 2020) and southernmost Mariana subduction zone (Zhu *et al.*, 2019, 2020; Li *et al.*, 2023; Chen *et al.*, 2025). The earthquake depths in the long term are still not well constrained.

In regions with limited seismic stations, various strategies have also been applied to improve the focal depth of shallow earthquakes. Waveform modeling of short-period (such as 5–15 s) teleseismic body waves is utilized to determine the source parameters of moderate-to-strong earthquakes in the Southwest Mariana rift (Zang *et al.*, 2025). Another effective approach is to extract depth-sensitive signals, such as the amplitude spectra of short-to-intermediate period (0.5–100 s) surface waves (Tsai and Aki, 1970; Fox *et al.*, 2012; He *et al.*, 2023; Somiah *et al.*, 2025) or depth phases such as *pP* and *sP* waves (Warren and Shearer, 2005; Stein and



Downloaded from pubs.geoscienceworld.org/ssa/srl/article-pdf/doi/10.1785/0220260037/8402433/srl-2026037.1.pdf by Chinese University Hong Kong user on 17 October 2026

Wiens, 2010; Wang *et al.*, 2017). The amplitude spectra of surface waves are highly depth sensitive, particularly for short-to-intermediate periods. He *et al.* (2023) demonstrated that the approach by utilizing optimal amplitude spectra of short-period (0.5–20 s) Rayleigh waves is applicable for sparse seismic station coverage at local distances. Somiah *et al.* (2025) further suggest that the sparse seismic network in Western and Central Africa can also resolve reliable source depths using short-period Rayleigh-wave amplitude spectra on even only one or a few seismic stations at regional distances (≤1000 km).

So far, the historical earthquake depths are poorly constrained, and there is a lack of systematic assessment of the source depth of shallow moderate-sized earthquakes in the Mariana region. In this study, we collect the seismic data at local and regional distances, then use the optimal period of short-period Rayleigh-wave amplitude spectra to determine the depths of earthquakes. We also adopt depth phase modeling to verify the estimated depth. We demonstrate the efficacy of this approach on shallow offshore earthquakes in subduction zones, and reassess the depth of shallow moderate-sized earthquakes in the Mariana subduction zone.

## Data and Methods

### Depth constrained by optimal period of short-period Rayleigh-wave amplitude spectra

Our study aims to assess the depth of shallow moderate-sized earthquakes that occurred in the Mariana subduction zone. We selected 101 events with magnitudes ranging from 4.5 to 5.9 and depth shallower than 30 km from the period 2010 to 2025. The seismograms (a length of 300 s starting from earthquake origin time) were downloaded from the Incorporated Research Institutions for Seismology (IRIS) data center (see Data and Resources) and were then preprocessed by removing the instrument response to ground displacement, removing the mean value, and detrending. We checked the seismograms and retained the seismograms with identifiable Rayleigh waves with signal-to-noise ratio (SNR) ≥3. Here, the SNR of the Rayleigh wave was calculated as a ratio of the energy within the selected time window to the energy of tailing noise. Assuming the group velocity of a Rayleigh wave is 1.8–4.0 km/s, the time window used for analysis is (distance/4.0 s, distance/1.8 s). The tailing noise window was taken as a 20 s segment after the signal.

The amplitude spectra of short-to-intermediate period Rayleigh waves are highly depth sensitive because their displacement decreases exponentially with increasing depth. It is pivotal to extract the optimal period corresponding to the maximum spectral amplitude of Rayleigh waves. We adopted the approach by He *et al.* (2023) for resolving earthquake depth. The first step was to determine the optimal period of Rayleigh wave recorded by each station (Fig. 2). We measured the amplitude spectra by performing multiple filter analysis using the "do mft" algorithm in the Computer Programs in Seismology (CPS) package (Herrmann, 2013). The optimal period was obtained by extracting the maximum spectral amplitude. We only retained earthquakes with highly consistent amplitude spectra on at least two stations (Fig. S1). Considering the sparse station coverage in the Mariana subduction zone, the final optimal period for each earthquake is calculated by averaging the measured optimal periods at available stations. The standard deviation of measured optimal periods is also calculated, which is used for evaluating uncertainties. We note that the standard deviation is influenced by variations in station azimuth and distance and should therefore be interpreted as an empirical spread rather than a formal uncertainty.

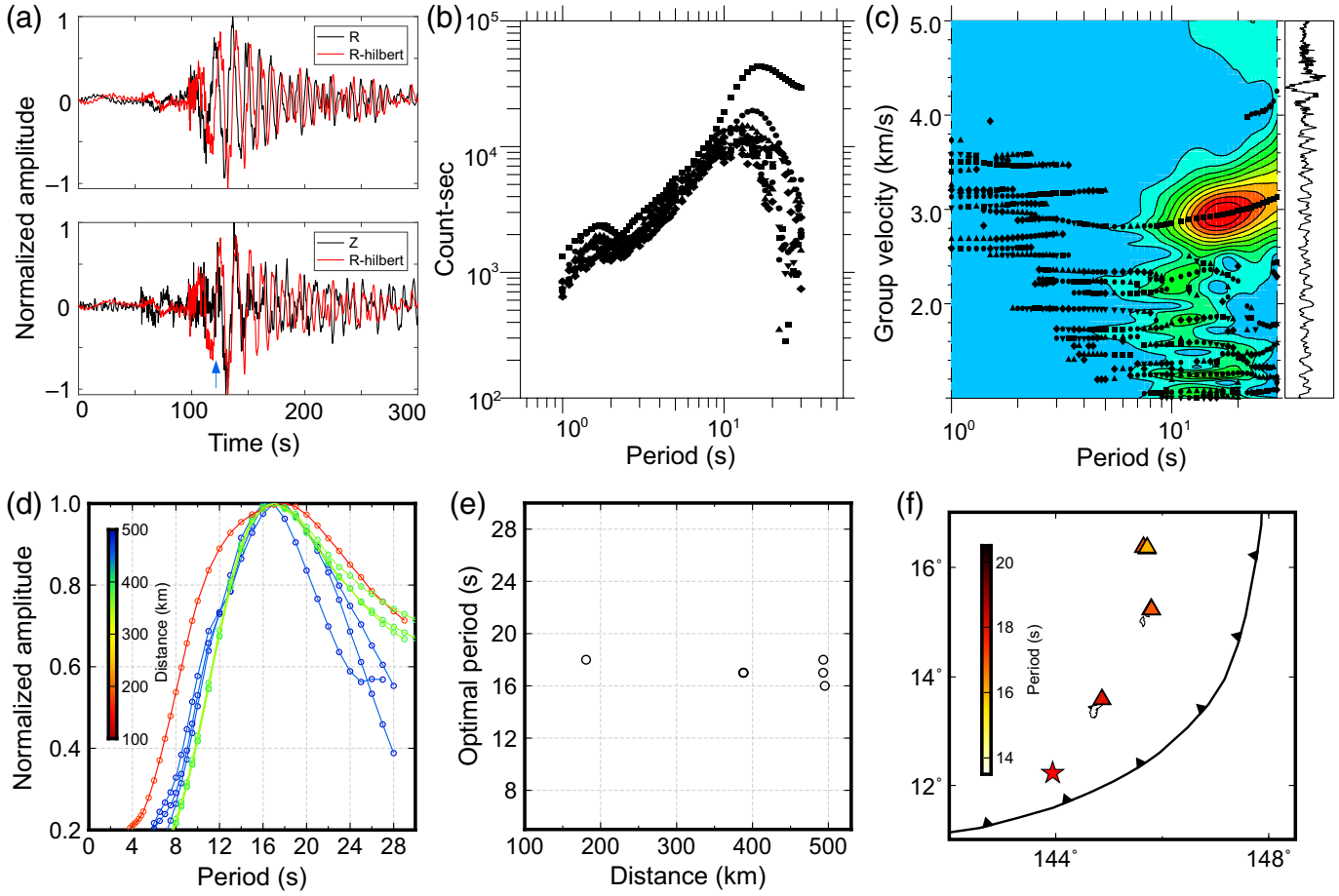
In the second step, we synthesized the spectra of fundamental-mode Rayleigh waves based on eigenfunctions for a depth range of 0–30 km (Fig. 3). A 1D velocity model of the central Mariana fore-arc in figure 2d from Cai *et al.* (2018) was used, because all stations sat on the arc islands. The effects of the 2D velocity model were tested in the Discussion section. As the majority of shallow earthquakes in this study were normal faulting or strike-slip faulting mechanisms, we assumed a normal faulting of a real earthquake (strike = 11°, dip = 42°, slip = −51°) and a vertical strike-slip faulting (strike = 0°, dip = 90°, slip = 0°), respectively. We simulated a receiver station at distances of 200 km (Fig. 3). Note that the impact of this receiver distance (Fig. 4) was described in the Discussion section. Theoretical amplitude spectra were then computed for azimuths ranging from 0° to 360° with an interval of 30°, from which the optimal periods were derived and then averaged over various azimuths. The averaged optimal periods of theoretical spectra for depths of 0–30 km exhibit almost linear increases with depth; however, the slope varies, being smaller for slower wave velocities and larger for faster wave velocities. Finally, the earthquake depth can be estimated based on the relationship between the optimal period and focal depth.

### Independent verification of source depth using the depth phase modeling

To further verify the estimated source depth, we chose the largest $M_w$ 5.9 earthquake and the 2013 $M_w$ 5.3 earthquake in Table S1, and then used depth phase modeling to constrain their source depth. The depth phases (e.g., *pP* and *sP*) are the surface-reflected *P* and *S* waves. The travel-time delay between the depth phases and the direct *P* phase is caused by the double travel in the region above the source. At teleseismic distance, the separation is very sensitive to the focal depth (Murphy, 2006; Stein and Wiens, 2010). Therefore, we downloaded teleseismograms at distances of 30°–90° from the IRIS data center. We adopted the frequency–wavenumber method (Zhu and Rivera, 2002) to compute Green's functions. During the modeling of depth phases, we generated synthetic seismograms at each station for focal depth in the range of 1–30 km with a 1 km interval. The cross-correlation coefficient (CCC)



Downloaded from pubs.geoscienceworld.org/ssa/srl/article-pdf/doi/10.1785/0220260037/8402433/srl-2026037.1.pdf by Chinese University Hong Kong user on 17 October 2026




between the observed data and synthetics was then computed, based on which the depth was estimated at each station (Fig. 5). We then averaged the depths across stations with CCC > 70% as the final depth and regarded the 95% confidence interval as uncertainty (Wang *et al.*, 2017).

## Results

Among the downloaded 101 earthquakes, many have recordings on only a few stations within a distance of 600 km. Eventually, we obtained source depths of 30 events in both the incoming and overriding plates (Fig. 1), with stable amplitude spectra on at least two stations using the "do mft" analysis. The results of the source parameters were summarized in Table S1. For all reassessed earthquakes in the entire region, we compared the source depths from our study with the IRIS and Global Centroid Moment Tensor (CMT; Ekström *et al.*, 2012) catalogs (Fig. 6). The difference between our resolved depths and the IRIS results ranges from −12.5 to 17.5 km, whereas the difference between our resolved depths and the Global CMT depths has a range of −7.5 to 12.5 km.

Taking the 30 March 2013, $M_w$ 5.2 event as an example (Fig. 2), the IRIS located the earthquake at a depth of 25.8 km, whereas the Global CMT placed the event at a depth of 12.9 km. According to the amplitude spectra analysis, the group velocity of Rayleigh waves exhibited obvious dispersion, with velocities ranging from 2.8 to 3.2 km/s. The group velocity was ∼3.0 km/s at a period of 20 s, which is consistent with observed dispersion from the OBS data (Cai *et al.*, 2018). The polarization analysis is performed with the Hilbert transform of radial component. The Hilbert-transformed radial component is approximately in phase with the vertical

**Figure 2.** Rayleigh-wave optimal period of the 30 March 2013 $M_w$ 5.2 event in the southern Mariana. (a) The vertical- and radial-component seismograms (black trace) at the DPS station with distance of 388 km. The red trace represents the Hilbert transform of radial component. The blue arrow marks the Rayleigh-wave arriving after ∼120 s, indicating group velocity ≤ 3.23 km/s. (b,c) Multiple filter analysis generating (b) spectral amplitudes and (c) group velocity dispersion of Rayleigh wave at the DPS station. The colors in the group velocity plot are scaled to the envelope amplitude at each filter period, with amplitude increasing from blue to red. The black symbols represent the chosen peaks from the stack after a 2D search over the group velocity—period grid. (d) Amplitude spectra for all stations with epicentral distances of 100–500 km. The color represents epicentral distance. (e) Variation of optimal periods with distance. (f) The optimal periods for all stations. The red star represents the earthquake, and the triangles show the stations. The color bar presents the optimal period at each station. The color version of this figure is available only in the electronic edition.



Downloaded from pubs.geoscienceworld.org/ssa/srl/article-pdf/doi/10.1785/0220260037/8402433/srl-2026037.1.pdf by Chinese University Hong Kong user on 17 October 2026

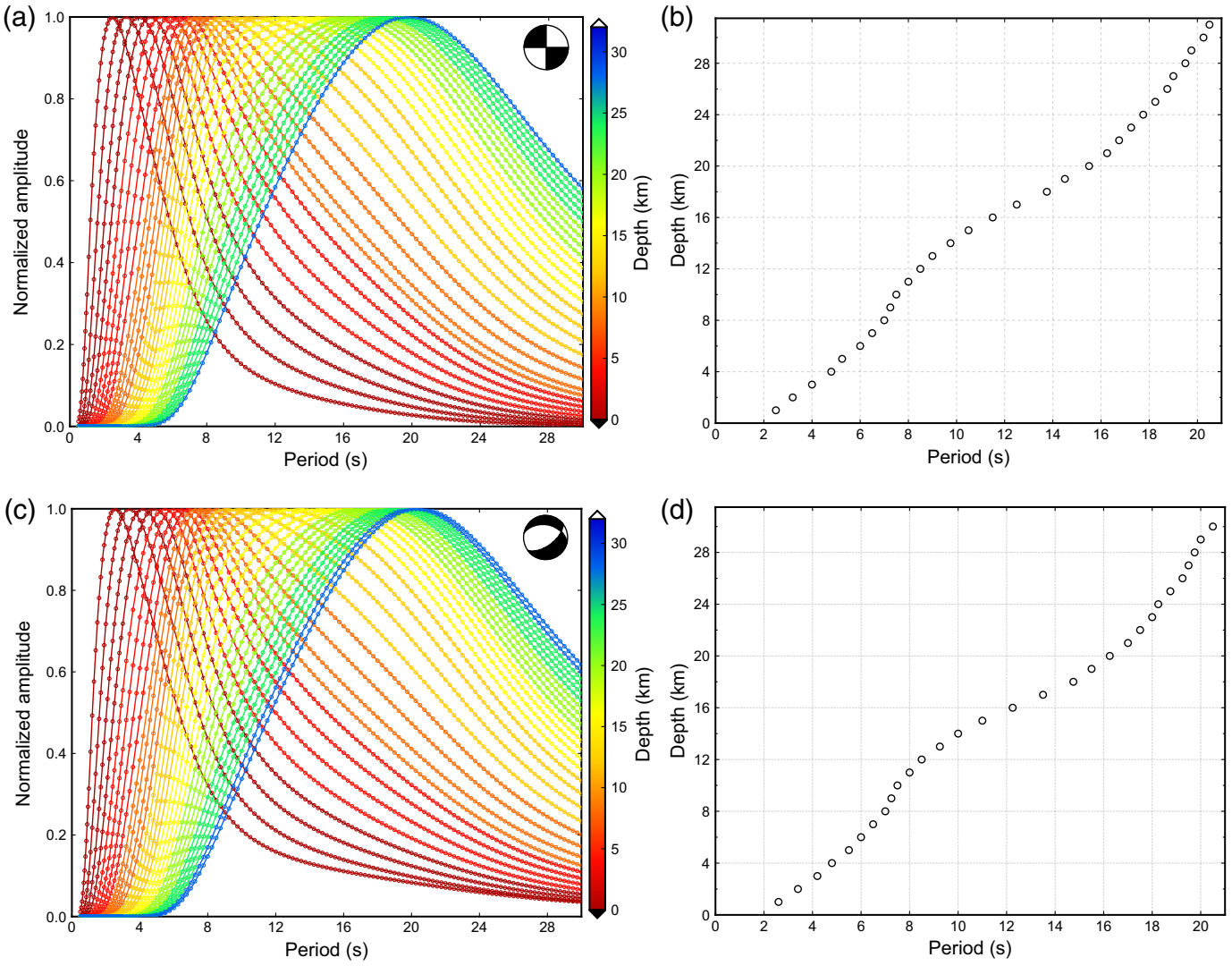



**Figure 3.** (a) Theoretical Rayleigh-wave amplitude spectra (normalized) for different source depths, with vertical strike-slip faulting (strike = 0°, dip = 90°, slip = 0°). The receiver station is located 200 km away with an azimuth of 45°. The velocity model refers to Cai *et al.* (2018) in the Mariana subduction zone. (b) Derived relationship between the focal depth and the optimal period. (c,d) Same for (a,b), but a normal-faulting earthquake (strike = 11°, dip = 42°, slip = −51°). The color version of this figure is available only in the electronic edition.

component, which confirms the correct identification of Rayleigh waves. The distance of 388 km and the arrival time of ∼120 s indicate a group velocity smaller than 3.23 km/s, which agrees with group velocities obtained from spectra analysis. The optimal periods for all stations ranged from 16 to 18 s, which shows slight variation with epicentral distance. Considering the sparse stations, we preferred to take the average value of optimal periods rather than fitting a linear trend. The average optimal period of this event was calculated to be 17.1 s, with a standard deviation of 0.69 s. Then, we estimated a focal depth of 22.6 km based on the averaged optimal period, and the uncertainty was ∼1.4 km stemming from the standard deviation.

For earthquakes in the outer-rise region of the incoming plate, we discovered that the earthquake focal depths with extensional faulting mechanisms extended to a depth of 24.4 km (event 2018-10-26T09_05_39) below the seafloor in the central Mariana, and to a depth of 22.5 km (event 2016-09-03T14_04_47) below the seafloor in northern Mariana. In comparison, the depth of extensional earthquakes was shallower than 20 km below the seafloor in southern Mariana (Fig. 1). The results are generally consistent with previous relocated earthquakes (Emry *et al.*, 2014) in the same region (Fig. 1b–d).

Depth phases were used to constrain the focal depth of the 26 October 2018 $M_w$ 5.9 event (Fig. 5). The averaged result across stations is 27.9 km, with 95% confidence interval of (27.6, 28.2) km. The stations show quite consistent depth, suggesting a robust depth of this event. The result of depth phase modeling is slightly larger than the depth of 24.4 ± 1.4 km using the



Downloaded from pubs.geoscienceworld.org/ssa/srl/article-pdf/doi/10.1785/0220260037/8402433/srl-2026037.1.pdf by Chinese University Hong Kong user on 17 October 2026

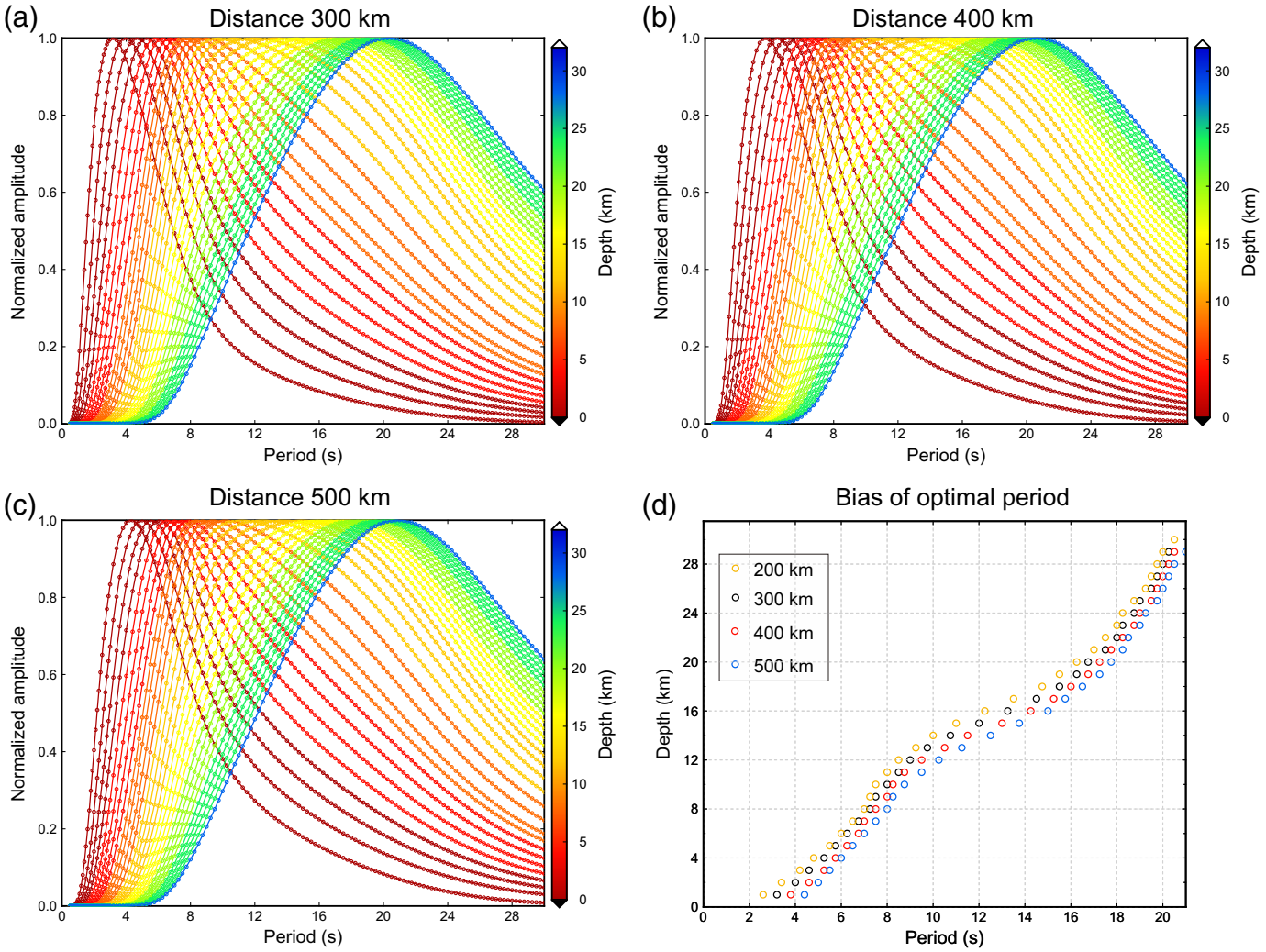



**Figure 4.** Testing the impact of receiver distances on optimal periods. (a–c) Theoretical Rayleigh-wave amplitude spectra (normalized) for different source depths, with a normal-faulting earthquake (strike = 11°, dip = 42°, slip = −51°). The receiver station is located at 300, 400, and 500 km. (d) Comparison of the derived optimal periods among the various receiver distances. The color version of this figure is available only in the electronic edition.

optimal period method. In comparison, the IRIS and Global CMT catalogs provide a fixed depth of 10 and 12 km, respectively. We also conducted a similar analysis for the 2013 $M_w$ 5.3 event (Fig. S2). The result of depth phase modeling indicates a focal depth of 18.8 km, which is 1.3 km larger than the focal depth of 17.5 km constrained by the optimal period method.

We further did optimal period analysis for three historical events during 1990–2011 and compared our results with independent depth estimates of events in Craig *et al.* (2014), in which the source parameters of outer rise earthquakes were determined by body-waveform modeling. There were a total of 13 events in the Mariana region documented in the supplementary table, but only 5 events among them had a magnitude <6.0 and depth <30 km (Craig *et al.*, 2014). As the events occurred during 1990–2011, only one station GUMO is available in the Mariana region before 2011. Finally, we only found three events with a distance <600 km to the GUMO station. Then, we conducted the amplitude spectra analysis and compared the results with Craig *et al.* (2014). The depth difference is 2.4 and 1.8 km for the 2005 and 1994 events, respectively (Table S2). However, for the 2003 event, our estimated depth (24.4 km) is significantly larger than 8 km in Craig *et al.* (2014). We considered that this large difference may stem from multiple possible factors, such as the lateral heterogeneity of velocity structure, only one station used in our study, or possible bias caused by preferential fitting of dominant frequencies during the waveform inversion in Craig *et al.* (2014).

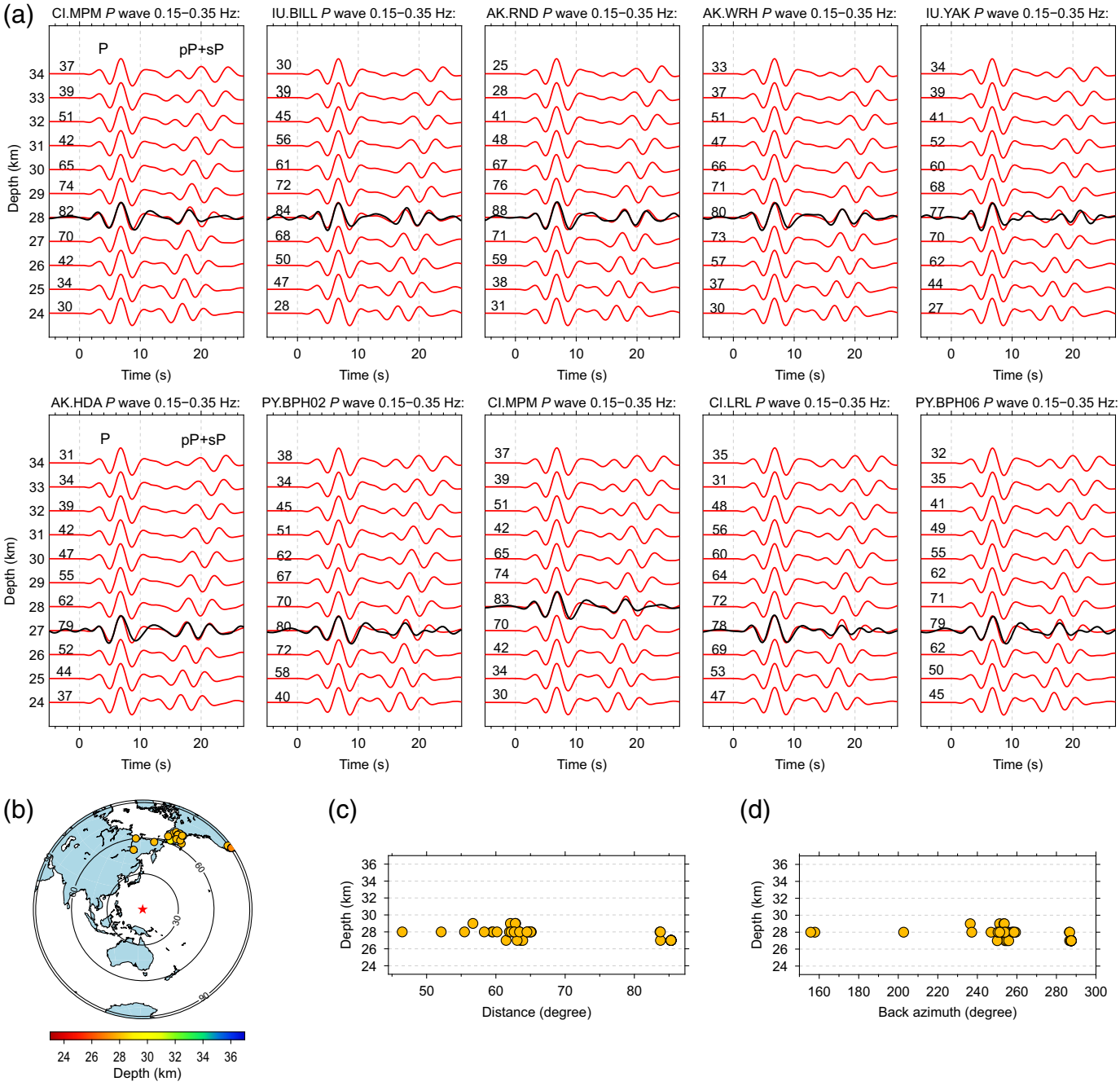
## Discussion

### Tectonic implications of the estimated depth of earthquakes

Precisely estimating the depths of moderate-sized earthquakes is crucial for tectonic and seismic studies. However, the global catalog has a fixed source depth of 10 km for many earthquakes in the Mariana subduction zone (Table S1, Fig. 6), which is



Downloaded from pubs.geoscienceworld.org/ssa/srl/article-pdf/doi/10.1785/0220260037/8402433/srl-2026037.1.pdf by Chinese University Hong Kong user on 17 October 2026




often considered to reflect the large uncertainty. The Global CMT catalog determines source parameters by fitting intermediate- to long-period (approximately 40–150 s) teleseismic body wave and surface waveforms, as well as longer-period (125–350 s) mantle wave signals (Ekström *et al.*, 2012). It provides relatively reliable estimates of magnitude and moment tensor but has limited resolution for shallow earthquake depths, with depths typically being fixed at a minimum of 12 km (Table S1, Fig. 6). According to our reassessed source depth of shallow moderate-sized earthquakes, the depth uncertainty of global catalogs can be as large as 15 km in the Mariana subduction zone. The large location uncertainties have also been reported by several studies based on OBS data in the

**Figure 5.** Focal depth constrained by depth phases for the 26 October 2018 $M_w$ 5.9 event. (a) The depth phases modeling of representative stations, with red and black curves representing synthetic and observed data, respectively. The synthetics are computed with source depth ranging from 24 to 34 km with an interval of 1 km. The observed data and synthetic seismograms are filtered to 0.15–0.35 Hz, and their cross-correlation coefficient (CCC) in percentage is marked on the right top of each trace. (b) Location of all available stations (dots) used in this study, colored by estimated source depth at each station. The best source depth at each station, sorted by (c) distance and (d) back azimuth, respectively. The color version of this figure is available only in the electronic edition.



Downloaded from pubs.geoscienceworld.org/ssa/srl/article-pdf/doi/10.1785/0220260037/8402433/srl-2026037.1.pdf by Chinese University Hong Kong user on 17 October 2026

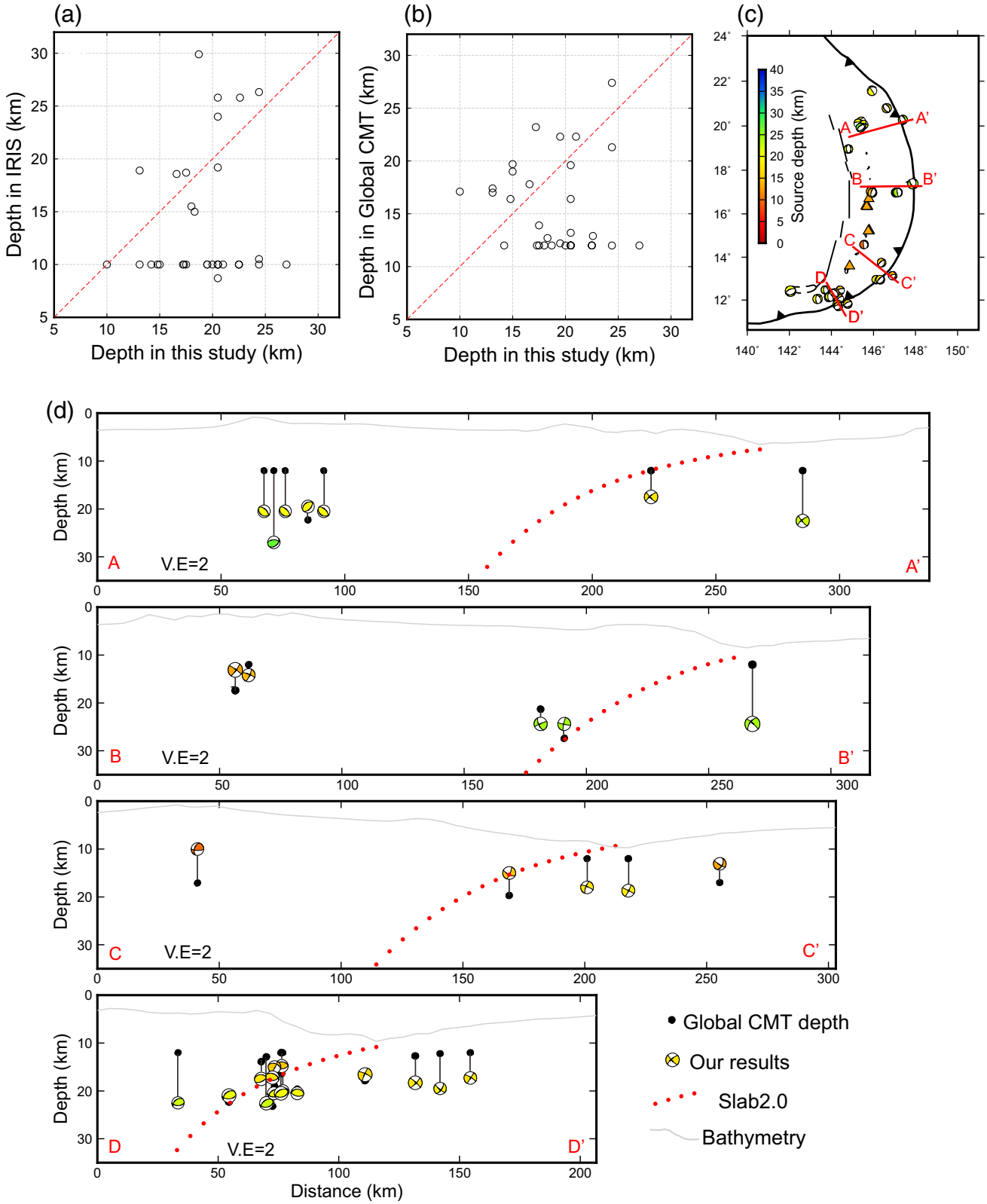



**Figure 6.** Comparing the source depth in this study with the depth in (a) Incorporated Research Institutions for Seismology (IRIS) catalog and (b) Global Centroid Moment Tensor (Global CMT) catalog. (c) Map view of the analyzed earthquakes (shown as focal mechanism plots) and location of four profiles (red lines marked with AA′, BB′, CC′, and DD′). (d) The cross-sectional views of comparing our source depths (focal mechanism plots) with Global CMT depths (black dots). The color version of this figure is available only in the electronic edition.



Downloaded from pubs.geoscienceworld.org/ssa/srl/article-pdf/doi/10.1785/0220260037/8402433/srl-2026037.1.pdf by Chinese University Hong Kong user on 17 October 2026

central (Emry *et al.*, 2011; Eimer *et al.*, 2020) and southern Mariana (Zhu *et al.*, 2019). Such large uncertainties may cause biases in results relying on global catalogs. Therefore, it is necessary to reassess the source depths in the Mariana region.

According to the newly obtained focal depths in the outer-rise region of the incoming plate, focal depths with extensional faulting mechanisms can extend to a depth of 24.4 km below the seafloor in the central Mariana, and to a depth of 22.5 km below the seafloor in northern Mariana. The results further evidence that normal faults can extend into the uppermost mantle at the Mariana trench-outer-rise bending region, through which water may transport into the mantle, thus leading to a pervasively serpentinized upper mantle in the Mariana subduction (Fryer *et al.*, 1999). The estimated results are generally consistent with previous relocated earthquakes using OBS data (Eimer *et al.*, 2020) and possible hydration depth extent of ~24 km below Moho indicated by low mantle velocities in the region (Cai *et al.*, 2018). In comparison, the depth of extensional earthquakes was shallower than 20 km in the southern Mariana (Fig. 6d), which is consistent with the predicted neutral plane of ~20 km beneath the Pacific plate near the southern Mariana trench axis (Emry *et al.*, 2014).

### Advantages of optimal period method and relevant influencing factors

It is efficient to use the optimal period of Rayleigh-wave amplitude spectra method in this region. Apart from the reason of sparse stations, there are other advantages of the Rayleigh-wave amplitude spectra method. In comparison with the location methods based on travel times, using amplitude spectra avoids trade-offs between the location and original times (Klein, 2002). Compared to the waveform inversion method, using amplitude spectra is not affected by preferential fitting of dominant frequencies (Fox *et al.*, 2012).

Although the short-period Rayleigh wave is sensitive to source depth and has certain advantages, the method has a strong dependency on the structure model used. Studies have demonstrated that the Earth's structural properties (such as velocity and attenuation) have inevitable influences on propagation and dispersion of surface waves, which affect depth estimation using the Rayleigh-wave amplitude spectra (Tsai and Aki, 1970; Fox *et al.*, 2012). Because of inaccurate propagation and dispersion characteristics using imprecise structure models, surface waves are not commonly used for estimating depth in regions with sufficient local seismic stations. Improvements in velocity models have facilitated more reliable studies on surface-wave sources. Previous studies suggest that the focal depth of small-to-moderate events can be well determined by optimal amplitude spectra of short-period Rayleigh waves in various on-land tectonic settings (He *et al.*, 2023; Somiah *et al.*, 2025).

During estimation of source depth, we adopt a 1D velocity model from the advanced velocity structure derived from Rayleigh-wave analysis of broadband OBS data (Cai *et al.*, 2018). Although lateral variation of velocity structure has not been considered, we think that the source depths have been significantly improved by using the optimal amplitude spectra method. As independently evidenced by the depth phase modeling of the $M_w$ 5.9 event, the depth is 27.9 km, which is slightly larger than the depth of 24.4 ± 1.4 km using the optimal period method. In comparison, global catalogs provide a fixed depth of 10 or 12 km for the event. The result of depth phase modeling of the 2013 $M_w$ 5.3 event indicates a focal depth of 18.8 km, which is similar to the focal depth of 17.5 km constrained by the optimal period method.

Considering 2D heterogeneities in the Mariana subduction zone, we investigated the influence of the 2D velocity model on this method. We used the high-precision spectral element method to perform waveform simulations (SPECFEM2D package; Komatitsch and Vilotte, 1998) with the representative 2D section velocity model derived from Rayleigh-wave analysis of broadband OBS data (Cai *et al.*, 2018). The modeled region ranges 0–300 km laterally and 0–60 km vertically (Fig. S3). The source was placed at 10, 15, and 20 km and a total number of 20 receivers were set on the surface. We then calculated the 2D synthetic seismograms and compared them with 1D synthetics. To suppress the complex source structural effects on wavefield excitation, we measured the optimal periods of the 2D and 1D broadband synthetics at the receivers far away from the source region. The differential optimal period was less than 1.0 s based on the current testing models.

To test the impact of receiver distances on the theoretical optimal period, we synthesized amplitude spectra at various distances (300, 400, and 500 km; Fig. 4), with a real normal-faulting earthquake with a focal mechanism of (strike = 11°, dip = 42°, slip = −51°). For a certain focal depth, the optimal period increases slightly with distance. The difference is within 2.0 s at distances 300, 400, and 500 km. Therefore, it is expected to take linear fits between the optimal period and distance for a dense network in an ideal condition. However, it is hard to fit the linear relationship if networks are scarce. Instead, taking the average of optimal periods is suggested for sparse networks.

We further investigated the azimuthal variation of optimal periods for different focal depths of 10 and 20 km (Fig. S4). The variations of optimal periods are within ±10 percent of the mean value, consistent with the previous testing result in He *et al.* (2023) for earthquakes on land. This implies the maximum uncertainty of 10% in the resolved depth, for example, 1 km uncertainty for a source at a depth of 10 km, 2 km uncertainty for a source at a depth of 20 km. For real cases, the uncertainty can be suppressed by averaging the optimal methods at stations of different azimuths.

## Conclusion

Accurately determining the focal depth of shallow earthquakes is challenging in the Mariana subduction zone because of



Downloaded from pubs.geoscienceworld.org/ssa/srl/article-pdf/doi/10.1785/0220260037/8402433/srl-2026037.1.pdf by Chinese University Hong Kong user on 17 October 2026

limited seismic stations. In this study, we adopt the optimal period of short-period Rayleigh-wave amplitude spectra to determine the depths of shallow moderate-sized earthquakes, based on seismic data at local and regional distances in the Mariana region. We select 101 events with magnitudes ranging from 4.5 to 5.9 and depths shallower than 30 km from the period 2010 to 2025. We finally estimate the source depths of 30 events among them, with consistent amplitude spectra on at least two stations. As an independent verification of the estimated source depth, we conduct depth phase modeling to constrain the source depth of the largest $M_w$ 5.9 earthquake. The depth phase modeling provides a depth of 27.9 ± 0.3 km, which is slightly deeper than the depth of 24.4 ± 1.4 km constrained by the optimal period method. The estimated depth significantly differs from the fixed depth of 10 and 12 km in the IRIS and Global CMT catalogs, respectively. Our results indicate that global catalogs have a serious deviation from the real source depth in the Mariana region. Therefore, attention should be paid to the large depth uncertainties in the global catalog of historical earthquakes, despite their potential to provide valuable insights into subduction processes. Adding constraints from short-period surface waves can be an efficient way to improve the source depth of shallow earthquakes from global catalogs, in regions with sparse seismic data.

## Data and Resources

The earthquake information and seismograms of earthquakes are downloaded from Incorporated Research Institutions for Seismology (IRIS) data center (https://www.iris.edu). The focal mechanisms are from the Global Centroid Moment Tensor (Global CMT) Project database (www.globalcmt.org/CMTsearch.html). Both websites were last accessed in May 2026. The Computer Programs in Seismology (CPS) package (Herrmann, 2013) is used for performing multiple filter analyses and synthesizing theoretical Rayleigh-wave spectra. The supplemental material for this article includes supporting tables of earthquake source parameters, depth phases modeling and comparison in amplitude spectra for 1D and 2D synthetics, and figures of the determination of Rayleigh-wave optimal period for all events (Fig. S5) in this study. These supporting tables and figures are only available online.

## Declaration of Competing Interests

The authors acknowledge that there are no conflicts of interest recorded.

## Acknowledgments

The authors thank the professional staff who maintain the seismic networks. Feedback provided by two anonymous reviewers improved the quality of this article and is much appreciated. This study is supported by National Natural Science Foundation of China (42406064, U2344221), National Key Research and Development Program of China (2023YFF0806400), Shandong Province Outstanding Youth Science Fund Project Overseas (2023HWYQ-099), Talent Program of the Chinese Academy of Sciences (E5KY40101L), Taishan Scholar Foundation of Shandong Province (tstp20230638), Hong Kong Research Grant Council Grants (Grant Numbers 14308523 and 14306122), and 1+1+1 CUHK-CUHK(SZ)-GDSTC Joint Collaboration Fund (2025A0505000082).

## References

Barklage, M., D. A. Wiens, J. A. Conder, S. Pozgay, H. Shiobara, and H. Sugioka (2015). P and S velocity tomography of the Mariana subduction system from a combined land-sea seismic deployment, *Geochem. Geophys. Geosys.* **16**, no. 3, 681–704, doi: 10.1002/2014GC005627.

Cai, C., D. A. Wiens, W. Shen, and M. Eimer (2018). Water input into the Mariana subduction zone estimated from ocean-bottom seismic data, *Nature* **563,** no. 7731, 389–392, doi: 10.1038/s41586-018-0655-4.

Chen, H., H. Yang, G. Zhu, M. Xu, J. Lin, and Q. You (2022). Deep Outer-rise faults in the southern Mariana subduction zone indicated by a machine-learning-based high-resolution earthquake catalog, *Geophys. Res. Lett.* **49,** no. 12, doi: 10.1029/2022gl097779.

Chen, H., G. Zhu, H. Yang, J. Zhang, S. Lu, C. Chen, J. Lin, and Y. Luo (2025). Along-strike variations in intermediate-depth seismicity in the southernmost Mariana subduction zone: Impact from the subduction of an oceanic plateau, *Tectonophysics* **913,** doi: 10.1016/j.tecto.2025.230875.

Craig, T. J., A. Copley, and J. Jackson (2014). A reassessment of outer-rise seismicity and its implications for the mechanics of oceanic lithosphere, *Geophys. J. Int.* **197,** no. 1, 63–89, doi: 10.1093/gji/ggu013.

Eimer, M., D. A. Wiens, C. Cai, D. Lizarralde, and H. Jasperson (2020). Seismicity of the incoming plate and forearc near the Mariana Trench recorded by ocean bottom seismographs, *Geochem. Geophys. Geosys.* **21,** no. 4, doi: 10.1029/2020gc008953.

Ekström, G., M. Nettles, and A. M. Dziewoński (2012). The global CMT project 2004–2010: Centroid-moment tensors for 13,017 earthquakes, *Phys. Earth Planet. In.* **200-201,** 1–9, doi: 10.1016/j.pepi.2012.04.002.

Emry, E. L., D. A. Wiens, and G. C. Daniel (2014). Faulting within the Pacific plate at the Mariana Trench: Implications for plate interface coupling and subduction of hydrous minerals, *J. Geophys. Res. Solid Earth* **119,** no. 4, 3076–3095, doi: 10.1002/2013JB010718.

Emry, E. L., D. A. Wiens, H. Shiobara, and H. Sugioka (2011). Seismogenic characteristics of the Northern Mariana shallow thrust zone from local array data, *Geochem. Geophys. Geosys.* **12,** no. 12, Q12008, doi: 10.1029/2011GC003853.

Fryer, P., C. G. Wheat, and M. J. Mottl (1999). Mariana blueschist mud volcanism: Implications for conditions within the subduction zone, *Geology* **27,** no. 2, doi: 10.1130/0091-7613(1999)027<0103:Mbmvif>2.3.Co;2.

Fox, B. D., N. D. Selby, R. Heyburn, and J. H. Woodhouse (2012). Shallow seismic source parameter determination using intermediate-period surface wave amplitude spectra, *Geophys. J. Int.* **191,** no. 2, 601–615, doi: 10.1111/j.1365-246X.2012.05612.x.

Gomberg, J. S., K. M. Shedlock, and S. W. Roecker (1990). The effect of S-wave arrival times on the accuracy of hypocenter estimation, *Bull. Seismol. Soc. Am.* **80,** no. 6A, 1605–1628, doi: 10.1785/bssa08006a1605.

Hayes, G. P., G. L. Moore, D. E. Portner, M. Hearne, H. Flamme, M. Furtney, and G. M. Smoczyk (2018). Slab2, a comprehensive subduction zone geometry model, *Science* **362,** no. 6410, 58–61, doi: 10.1126/science.aat4723.



Downloaded from pubs.geoscienceworld.org/ssa/srl/article-pdf/doi/10.1785/0220260037/8402433/srl-2026037.1.pdf by Chinese University Hong Kong user on 17 October 2026

He, E., X. Qiu, Y. Li, I. Grevemeyer, M. Xu, M. Zhao, Y. Wang, and C. Chen (2025). Strong serpentinization and hydration in the subducting plate of the Southern Mariana Trench: Insights from Vp/Vs ratios, *Geophys. Res. Lett.* **52,** no. 6, doi: 10.1029/2024gl113792.

He, X., P. Zhang, S. Ni, R. Chu, W. Wu, and K. Zheng (2023). Automatic determination of focal depth with the optimal period of Rayleigh wave amplitude spectra at local distances, *Geophys. J. Int.* **235,** no. 2, 1681–1696, doi: 10.1093/gji/ggad326.

Herrmann, R. B. (2013). Computer programs in seismology: An evolving tool for instruction and research, *Seismol. Res. Lett.* **84,** no. 6, 1081–1088, doi: 10.1785/0220110096.

Klein, F. W. (2002). User's guide to HYPOINVERSE-2000, a Fortran program to solve for earthquake locations and magnitudes, *US Geol. Surv. Open-File Rept. 2002-171*, 123 pp.

Komatitsch, D., and J.-P. Vilotte (1998). The spectral element method: An efficient tool to simulate the seismic response of 2D and 3D geological structures, *Bull. Seismol. Soc. Am.* **88,** no. 2, 368–392, doi: 10.1785/bssa0880020368.

Li, D., C. Chen, H. Zhang, Y. Wang, and S. Wu (2023). Preprocessing of passive-source ocean-bottom seismometer data in the Mariana subduction zone, *Geophys. Prospect.* **72,** no. 4, 1470–1485, doi: 10.1111/1365-2478.13372.

Mark, H. F., D. Lizarralde, and D. A. Wiens (2023). Constraints on bend-faulting and mantle hydration at the Marianas trench from seismic anisotropy, *Geophys. Res. Lett.* **50,** no. 10, doi: 10.1029/2023gl103331.

Murphy, J. R. (2006). Improved focal-depth determination through automated identification of the seismic depth phases pP and sP, *Bull. Seismol. Soc. Am.* **96,** no. 4A, 1213–1229, doi: 10.1785/0120050259.

Peng, Z., X. Lei, Q.-Y. Wang, D. Wang, P. Mach, D. Yao, A. Kato, K. Obara, and M. Campillo (2024). The evolution process between the earthquake swarm beneath the Noto Peninsula, Central Japan and the 2024 M 7.6 Noto Hanto earthquake sequence, *Earthq. Res. Adv.* doi: 10.1016/j.eqrea.2024.100332.

Qian, Y., X. Chen, W. Wu, S. Wei, S. Ni, M. Xu, Y. Qin, Y. Nakamura, Y. Zhou, and D. Sun (2024). Patterns of causative faults of normal earthquakes in the fluid-rich outer rise of Northeastern Japan, constrained with 3D teleseismic waveform modeling, *J. Geophys. Res. Solid Earth* **129,** no. 6, doi: 10.1029/2024jb028740.

Shiobara, H., H. Sugioka, K. Mochizuki, S. Oki, T. Kanazawa, Y. Fukao, and K. Suyehiro (2010). Double seismic zone in the North Mariana region revealed by long-term ocean bottom array observation, *Geophys. J. Int.* **183,** no. 3, 1455–1469, doi: 10.1111/j.1365-246X.2010.04799.x.

Somiah, J., S. Ni, and X. He (2025). Reassessment of focal depth estimates of small-to-moderate magnitude continental earthquakes in Western to Central Africa with the optimal period of Rayleigh wave amplitude spectra using sparse regional seismic data, *Phys. Earth Planet. In.* **360,** doi: 10.1016/j.pepi.2025.107322.

Stein, S., and D. A. Wiens (2010). Depth determination for shallow teleseismic earthquakes: Methods and results, *Rev. Geophys.* **24,** no. 4, 806–832, doi: 10.1029/RG024i004p00806.

Stern, R. J., M. J. Fouch, and S. L. Klemperer (2003). An overview of the Izu-Bonin-Mariana subduction factory, in *Inside the Subduction Factory*, J. Eiler (Editor), Vol. 138, American Geophysical Union, 175–222, doi: 10.1029/138gm10.

Suzuki, R., N. Uchida, W. Zhu, G. C. Beroza, T. Nakayama, K. Yoshida, G. Toyokuni, R. Takagi, R. Azuma, and A. Hasegawa (2025). The forearc seismic belt: A fluid pathway constraining down-dip megathrust earthquake rupture, *Science* **389,** no. 6756, 190–194, doi: 10.1126/science.adt6389.

Tsai, Y.-B., and K. Aki (1970). Precise focal depth determination from amplitude spectra of surface waves, *J. Geophys. Res.* **75,** no. 29, 5729–5744, doi: 10.1029/JB075i029p05729.

Wang, K., and J. He (2008). Effects of frictional behavior and geometry of subduction fault on coseismic seafloor deformation, *Bull. Seismol. Soc. Am.* **98,** no. 2, 571–579, doi: 10.1785/0120070097.

Wang, X., S. Wei, C. Morales-Yáñez, Z. Duputel, L. Chen, T. Hao, and L. Zhao (2024). Plate interface geometry complexity and persistent heterogenous coupling revealed by a high-resolution earthquake focal mechanism catalog in Mentawai, Sumatra, *Earth Planet. Sci. Lett.* **637,** doi: 10.1016/j.epsl.2024.118726.

Wang, X., S. Wei, and W. Wu (2017). Double-ramp on the Main Himalayan Thrust revealed by broadband waveform modeling of the 2015 Gorkha earthquake sequence, *Earth Planet. Sci. Lett.* **473,** 83–93, doi: 10.1016/j.epsl.2017.05.032.

Warren, L. M., and P. M. Shearer (2005). Using the effects of depth phases on P-wave spectra to determine earthquake depths, *Bull. Seismol. Soc. Am.* **95,** no. 1, 173–184, doi: 10.1785/0120030251.

Zang, C., M. Xu, S. Ni, and W. Wu (2025). Improved source parameter estimation of moderate-sized earthquakes in the Southwest Mariana Rift and its implications for arc deformation mechanisms, *Sci. China Earth Sci.* doi: 10.1007/s11430-024-1576-6.

Zhang, J. H., X. Wang, C. Cai, Y. Wang, J. Yang, and X. Huang (2025). Seismic imaging of upper mantle serpentinization and ponded melt at the boundary of the lithosphere and asthenosphere in the central Mariana subduction zone, *Geophys. Res. Lett.* **52,** no. 23, doi: 10.1029/2025gl119716.

Zhang, Y., M. Xu, Z. Xiao, Y. Zhou, C. Yu, J. Lin, H. Yang, and X. Qiu (2024). Ambient noise interferometry using ocean bottom seismometer data from active source experiments conducted in the southernmost Mariana Trench, *J. Geophys. Res. Solid Earth* **129,** no. 3, doi: 10.1029/2023jb027043.

Zhu, G., J. Lin, H. Yang, and Q. You (2020). Determining the orientation of ocean-bottom seismometers on the seafloor and correcting for polarity flipping via polarization analysis and waveform modeling, *Seismol. Res. Lett.* **91,** no. 2A, 814–825, doi: 10.1785/0220190239.

Zhu, G., D. A. Wiens, H. Yang, J. Lin, M. Xu, and Q. You (2021). Upper Mantle hydration indicated by decreased shear velocity near the Southern Mariana Trench from Rayleigh wave tomography, *Geophys. Res. Lett.* **48,** no. 15, doi: 10.1029/2021gl093309.

Zhu, G., H. Yang, J. Lin, Z. Zhou, M. Xu, J. Sun, and K. Wan (2019). Along-strike variation in slab geometry at the southern Mariana subduction zone revealed by seismicity through ocean bottom seismic experiments, *Geophys. J. Int.* **218,** no. 3, 2122–2135, doi: 10.1093/gji/ggz272.

Zhu, L., and L. A. Rivera (2002). A note on the dynamic and static displacements from a point source in multilayered media, *Geophys. J. Int.* **148,** no. 3, 619–627, doi: 10.1046/j.1365-246X.2002.01610.x.

**Manuscript received 20 January 2026**
**Published online 12 October 2026**



Downloaded from pubs.geoscienceworld.org/ssa/srl/article-pdf/doi/10.1785/0220260037/8402433/srl-2026037.1.pdf by Chinese University Hong Kong user on 17 October 2026